Available online at www.sciencedirect.com
ScienceDirect
Trans. Nonferrous Met. Soc. China 33(2023) 36−45
Transactions of Nonferrous Metals Society of China
www.tnmsc.cn

New method and mechanism for quickly obtaining quenching sensitivity temperature range of 7055 aluminum alloy

Xiao-fei SHENG[1,2], Cun-xiao HE[3,4], Ya-juan CHENG[5], Xiao-xiao RAO[2], Guo-ai HE[3,4]

1. School of Materials Science and Engineering, Central South University, Changsha 410083, China;
2. School of Materials Science and Engineering, Hubei University of Automotive Technology, Shiyan 442002, China;
3. Light Alloy Research Institute, Central South University, Changsha 410083, China;
4. State Key Laboratory of High Performance Complex Manufacturing, Central South University, Changsha 410083, China;
5. School of Physics and Materials Science, Guangzhou University, Guangzhou 510006, China

Received 22 October 2021; accepted 7 March 2022

Abstract: An alternating temperature heat treatment (ATHT) method with time-saving and resource-saving advantages was employed to measure the quenching sensitivity temperature range of the spray-deposited 7055 aluminum alloy based on hardness and electrical conductivity. Additionally, the microstructure evolution during ATHT was characterized by transmission electron microscopy (TEM). It was found that during ATHT of the 7055 alloy, the solute atoms precipitated, grew, and redissolved as the temperature increased. When the temperature reached 200 °C, the hardness of the alloy increased sharply, and the electrical conductivity increased modestly. As the temperature was increased above 400 °C, the electrical conductivity of this alloy declined rapidly and the solute atoms in the alloy redissolved quickly. Meanwhile, the η' strengthening phase in the alloy gradually evolved into the η equilibrium phase. By analyzing the hardness and electrical conductivity curves, the temperature range of quenching sensitivity for the current alloy was 200−400 °C, which was consistent with the results measured by the traditional graded heat preservation method.

Key words: aluminum alloy; alternating temperature heat treatment; quenching sensitivity temperature range; microstructure evolution

1 Introduction

As a classical structural material, 7055 aluminum alloy materials have been widely used in aerospace, transportation, and other fields due to their combined excellent thermal conductivity, corrosion resistance, weldability, and high specific strength [1−3]. Currently, research on 7055 aluminum alloy mainly focused on heat treatment processes [4,5], thermal deformation behavior [6,7], corrosion resistance [8,9], welding performance [10,11], and quenching sensitivity [12,13]. As a heat-treatable strengthening alloy, solution heat treatment, quenching, and aging are indispensable processes for obtaining structures with excellent mechanical properties [14]. Quenching sensitivity is an important factor that determines the properties of alloys during heat treatment. Therefore, determining the quenching sensitivity temperature range is extremely important for designing heat treatment parameters and obtaining the best performance of the alloy.

The quenching sensitivity of aluminum alloys has been widely studied based on the interrupted quenching method [15] and end-quench test [16].

Corresponding author: Guo-ai HE, Tel: +86-13117418436, Fax: +86-731-88830938, E-mail: heguoai@csu.edu.cn
DOI: 10.1016/S1003-6326(22)66088-6

In addition, analyzing time−temperature transformation (TTT) and time−temperature−property (TTP) curves during isothermal treatment is practical method for characterizing quenching sensitivity [17−20]. However, these methods required complicated and tedious processes. Moreover, they produced a substantial burden and required additional time for industrial production. In this work, we introduced a time-saving and resource-saving scheme to obtain the temperature range of quenching sensitivity.

In this work, we developed a short routine that utilized a low-energy-consumption homogenizing process. To obtain the temperature range of quenching sensitivity, this routine relied on a novel alternating temperature heat treatment (ATHT) method, which did not interrupt the quenching process. According to the new ATHT method, we determined the critical temperature region of the quenching sensitivity for the 7055 aluminum alloy. The microstructure evolution and corresponding mechanism in the 7055 aluminum alloy after ATHT were also illustrated.

2 Experimental

2.1 Material

The 7055 aluminum alloy used in this work was melted via the spray-deposition method (SFZD−5000, Jiangsu Haoran Inc., Zhenjiang, China). The key parameters used in the spray deposition of the AlZnMgCu alloy were as follows: pouring temperature of 780−950 °C, atomization gas rate of 20−35 m^3/min, metal flow fate of 8−55 kg/min, gas-to-metal ratio of (0.5−2):1, atomization gas pressure of 0.5−1 MPa, spray angle of 25°−35°, deposition distance of 150−290 mm, and the substrate rotation rate of 100−200 r/min. After spray deposition, the ~20 mm-thick surface layer was mechanically removed. The nominal composition of the 7055 aluminum alloy is listed in Table 1. Specifically, the content of elemental Zn was 8.31 wt.%, and the total content of Zn, Mg, and Cu in the alloy was more than 12.8 wt.%. Meanwhile, the ratio of Zn/Mg, which would affect quenching sensitivity, was 4.015:1. The Fe and Si impurities were effectively controlled and their sum was less than 0.14 wt.%.

Table 1 Composition of spray-deposited 7055 aluminum alloys (wt.%)

Al	Zn	Mg	Cu	Zr	Fe	Si
Bal.	8.31	2.07	2.46	0.12	0.078	0.056

2.2 Methods

First, the specimens were cut from the billet and subjected to solid solution treatment at 470 °C for 60 min. Afterward, they were quenched instantly in water within 2 s. Then, multiple specimens (usually 25−27) were placed in an electric furnace at room temperature (25 °C) and heated up at a rate of 10 °C/min to different target temperatures (25 °C, 60 °C, 80−460 °C with step intervals of 20 °C, and 470 °C). Afterward, all of the specimens were quenched instantly in water to maintain their microstructure at elevated temperatures. Finally, the specimens were subjected to subsequent hardness and electrical conductivity tests. Figure 1 shows the schematic diagram of the ATHT process.

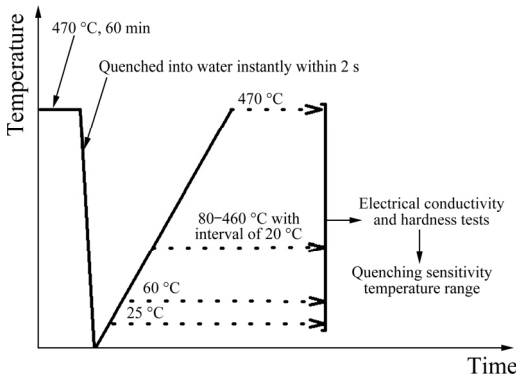

Fig. 1 Schematic diagram of ATHT process

Hardness measurements were conducted with an HV−5 hardness testing machine (Laizhou Huayin Testing Instrument Co., Ltd., Laizhou, China), with a load of 2 kg for 15 s. In this work, five independent measurements were carried out and the hardness was averaged by five data points. Microstructure observations were carried out on a TECNAI G2 F20 transmission electron microscope (FEI Company, Hillsboro, OR, USA) at an operation voltage of 200 kV. To improve experimental accuracy, at least three samples were tested under the same heat treatment conditions. The electrical conductivity tests were performed on a D60K digital metal conductivity testing apparatus with a measurement accuracy of about ±1%.

3 Results

3.1 Hardness curve and electrical conductivity curve

The hardness and electrical conductivity curves of the as-quenched 7055 aluminum alloy after the ATHT process are shown in Figs. 2 and 3, respectively.

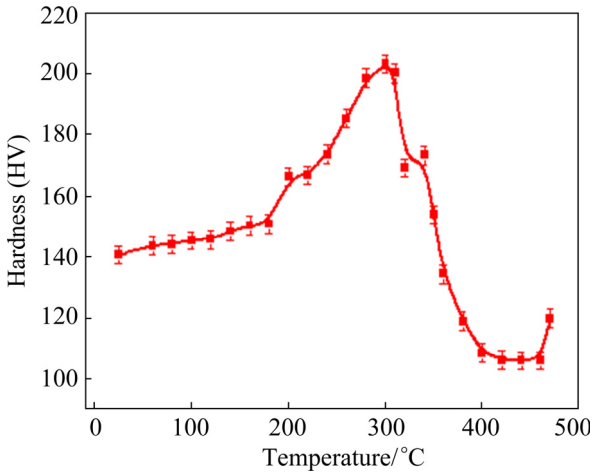

Fig. 2 Hardness curve of spray-deposited 7055 aluminum alloy during ATHT

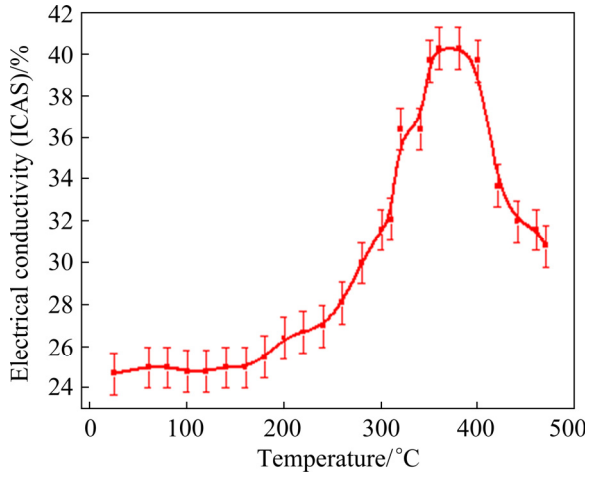

Fig. 3 Electrical conductivity curve of spray-deposited 7055 aluminum alloy during ATHT

As illustrated in Fig. 2, the hardness of this alloy was about HV 140 at room temperature, and it increased gradually during the initial stage. When the temperature was increased to 200 °C, the hardness increased gradually from HV 140 to 150. When the temperature exceeded 200 °C, the hardness increased rapidly to HV 167 at 210 °C. Then, it increased continuously with temperature and reached HV 203 at 310 °C. Afterward, the hardness started to decline with further increase in temperature up to 400 °C. Between 400 and 460 °C, the hardness was stable. When the samples were heated to the solution temperature (470 °C), the hardness of the quenched sample increased again and the value reached HV 119, which was HV 13 greater than the value at 460 °C.

As shown in Fig. 3, the electrical conductivity of the current alloy was stable at ~25.0% (ICAS) of the initial stage (below 160 °C). Subsequently, the electrical conductivity increased with increasing temperature and the value reached 26.7% (ICAS) at 220 °C. When the temperature was increased to 360 °C, the electrical conductivity reached a peak value of 40.3% (ICAS). Beyond 400 °C, the electrical conductivity started to drop rapidly until the end of the ATHT process. Thus, the electrical conductivity was 30.8% (ICAS) at 470 °C.

3.2 Microstructure evolution

The samples annealed at 60, 200, 310 and 470 °C were selected for transmission electron microscopy (TEM) characterization, which could characterize the microstructure evolution during the ATHT process. The corresponding results are shown in Figs. 4−7.

As shown in Fig. 4, except for Al_3Zr, no other

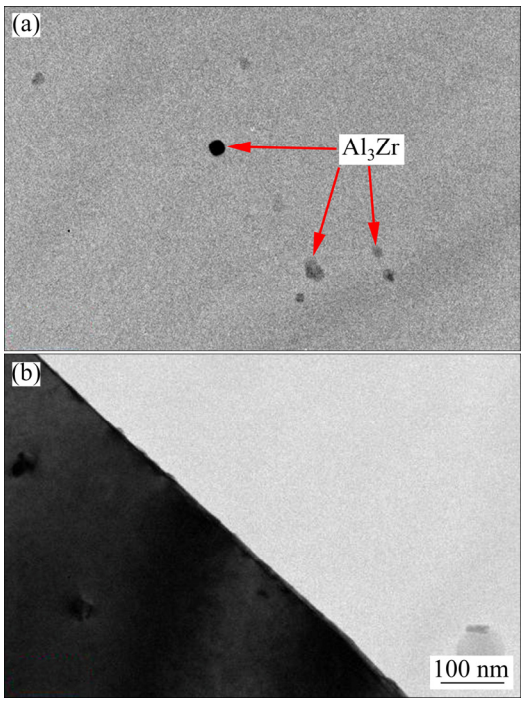

Fig. 4 TEM images of spray-deposited 7055 aluminum alloy after ATHT at 60 °C: (a) Inside grains; (b) On grain boundary

obvious second-phase particles were discovered inside the grains and on the grain boundaries. When the temperature was increased to 200 °C, no extra second phase was observed, and only Al_3Zr particles were observed inside the grains, as shown in Fig. 5(a). However, particles with a length of ~10 nm precipitated along the grain boundaries, as clearly observed in Fig. 5(b). Figure 5(c) shows the selected diffraction spot (SADP) corresponding to the center of Fig. 5(a), indicating that the Al_3Zr particles were formed along the $[110]_{Al}$ crystallographic orientation.

Figure 6 shows the TEM images of the spray-deposited 7055 aluminum alloy after ATHT at 310 °C, and Fig. 6(c) shows the selected diffraction spot corresponding to the central region of Fig. 6(a). It was observed that the η' phase, η phase, and Al_3Zr particles precipitated in this alloy when the temperature was increased to 310 °C. As shown in Fig. 6(a), the η and η' phases were dispersedly distributed inside the grains. Figure 6(b) demonstrates that the second phase along the grain boundary grew to a size of 50−100 nm at 310 °C, which was larger than that at 200 °C. This proved that the η' phase was the predominant strengthening precipitate of the 7055 aluminum alloy, which led to significant improvements in the properties of the 7055 aluminum alloy. When the temperature was increased to 470 °C, a rod-shaped η phase, with 50 nm × 100 nm in size, was apparently found in the alloy, as shown in Fig. 7(a). In addition, many particles along the grain boundary accumulated in an area of 30 nm × (30−50) nm × 50 nm in size.

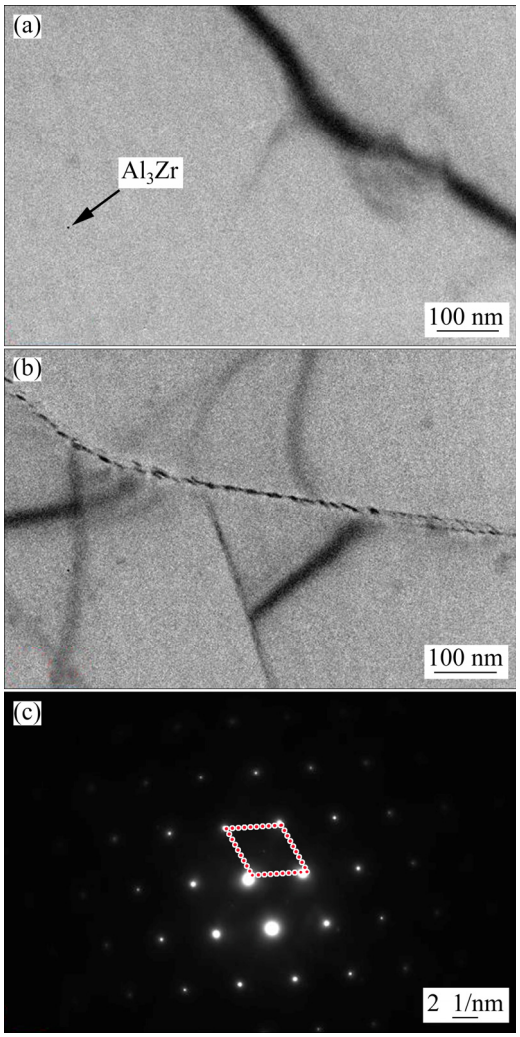

Fig. 5 TEM images of spray-deposited 7055 aluminum alloy after ATHT at 200 °C: (a) Inside grains; (b) On grain boundaries; (c) SADP patterns of different precipitations along $[110]_{Al}$

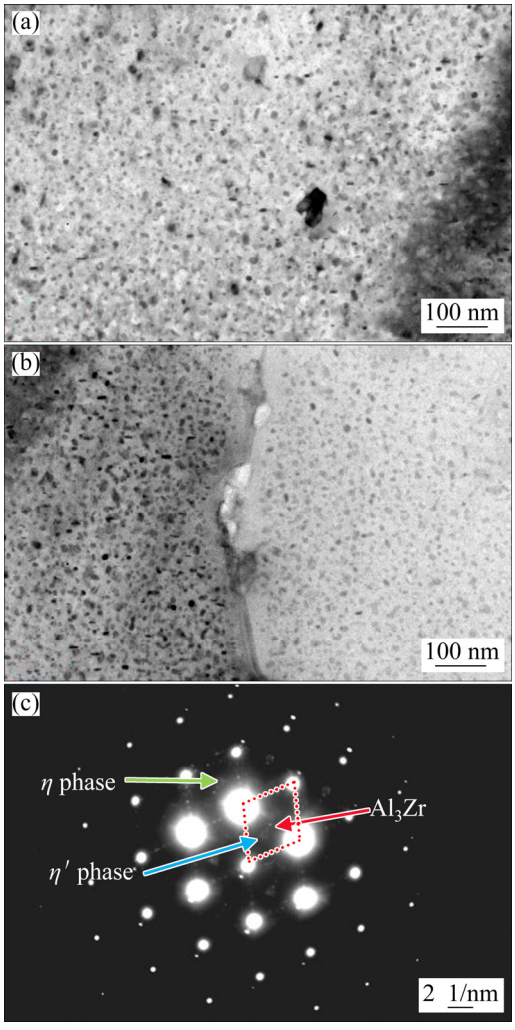

Fig. 6 TEM images of spray-deposited 7055 aluminum alloy after ATHT at 310 °C: (a) Inside grains; (b) On grain boundaries; (c) SADP patterns of different precipitations along $[110]_{Al}$

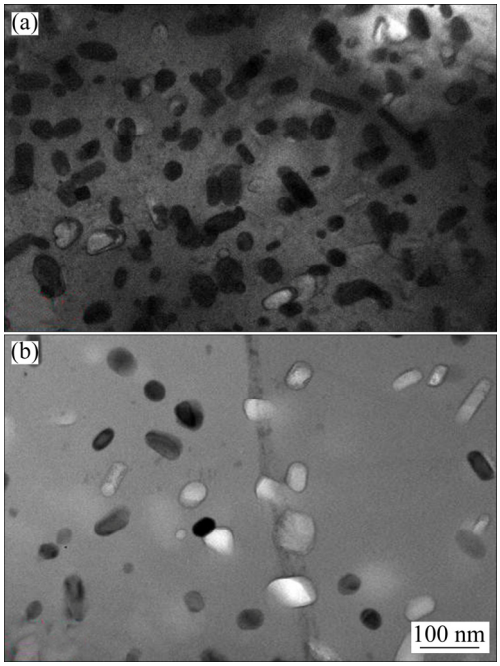

Fig. 7 TEM images of spray-deposited 7055 aluminum alloy after ATHT at 470 °C: (a) Inside grains; (b) On grain boundaries

4 Discussion

4.1 Performance variations

The spray-deposited 7055 aluminum alloy was an aging strengthening alloy that would evolve to a uniform single-phase supersaturated solid solution after solid solution treatment at 470 °C for 1 h. However, this state was unstable as the atom solutes in the matrix easily precipitated, forming a GP region or second phase. Therefore, during ATHT, the solute atoms in the homogeneous single-phase supersaturated solid solution had a tendency to precipitate. This has been investigated by previous studies, which showed that the temperature could significantly affect the rate of this process [21].

When the temperature was below 200 °C, the hardness of the alloy was improved slightly. The hardness of the alloy in this study, which was treated at 180 °C, was about HV 10 larger than that of the alloy treated at room temperature. At room temperature, the driving force was too small to trigger the precipitation of solute atoms from the supersaturated solid solution. In this condition, the precipitation of solute atoms in the matrix and the nucleation of second-phase particles were constrained, resulting in relatively unchanged electrical conductivity in this temperature range.

When the temperature was increased to above 200 °C, a sufficient driving force was achieved, allowing the solute atoms to precipitate. As a result, the supersaturated solid solution started to decompose and a strengthened phase was formed, which resulted in the rapid increase in hardness with temperature. Meanwhile, as precipitation progressed, the alloy matrix was purified, which weakened the scattering of electrons; thus, the electrical conductivity of the alloy started to increase.

As the temperature was increased to above 310 °C, the η' phase, one of the main strengthening phases of 7055 aluminum alloy, was found inside the grains, as presented in Fig. 6(a). This led to a further increase in hardness. However, with further increase in temperature, the precipitation rate of the atom solutes increased, resulting in an increased electrical conductivity slope compared to that at low temperatures.

With a continuous increase in temperature up to 360 °C, the electrical conductivity of this alloy reached its highest value with a small plateau. Above 400 °C, the electrical conductivity started to decline quickly, which indicated that the precipitated solute atoms began to redissolve into the matrix at high temperatures. Correspondingly, the hardness of the alloy decreased to HV 134. By increasing the temperature and prolonging the heat treatment time, the η' phase in the alloy evolved into the η phase. However, due to the incoherent relationship between the η phase and the matrix, the strengthening effect was weaker than that of the η' phase (semi-coherent with the matrix), resulting in a gradual decrease in hardness.

In addition, as presented in Figs. 2 and 3, when the temperature was above 400 °C, the precipitates started to redissolve into the matrix, resulting in a reduction in electrical conductivity. Between 400 and 460 °C, the solute atoms redissolved into the matrix, which induced solid solution strengthening. However, the solution strengthening effect was offset by the decrease in strength caused by the evolution from η' to η phases. However, the effect of solid solution strengthening was limited, as it could not completely compensate for the decrease in strength caused by phase transformation. As a result, the hardness declined continuously between 400 and 460 °C.

At 460 °C, the hardness of the alloy was as

low as HV 106, indicating that the strengthening effect of the η phase was weaker compared with the solid solution. When the temperature was increased to 470 °C, the strength of the alloy started to increase again due to the solid solution effect. At 470 °C, the extreme fine strengthening precipitates were almost redissolved in the matrix, as shown in Fig. 7. In this case, solid solution strengthening provided a positive effect for improving hardness, resulting in a reverse increase in hardness at 470 °C.

4.2 Evolution of precipitation

Precipitation strengthening was the dominant strengthening mechanism in the 7055 aluminum alloy. During ATHT, the commonly accepted precipitation sequence in 7055 aluminum alloys follows supersaturated solid solution (SSSS) → atom clusters → GP regions → η' precipitates → η precipitates [22,23]. During the ATHT process, the solute atoms precipitated, grew, and redissolved as the temperature was increased. It has been well documented that the stability of the supersaturated solid solution, the morphology, and the types of dispersoids and grain structures are three main factors that influence quenching sensitivity [24−26]. During the initial stage of ATHT, no other second-phase particles appeared in the matrix, except for Al_3Zr particles. These particles could efficiently inhibit the recrystallization process and refine the grain structure [27].

When the temperature was increased to 200 °C, the atom solutes in the supersaturated solid solution started to precipitate quickly from the matrix. The grain boundary, with high interfacial energy and strong nucleation tendency, would act as an effective site for quench-induced precipitation. As a result, the η' phase, which had a length of 10 nm, continuously precipitated and was distributed on the grain boundaries. When the temperature was increased to 310 °C, a considerable amount of short-rod-shaped η phase was formed both on the grain boundaries and inside the grains, as shown in Fig. 6. As the temperature continued to increase, more η phases gradually precipitated. At the same time, the η phase continued to absorb Mg and Zn atoms in the matrix, resulting in a significant decline in the concentration of solute atoms and vacancies.

As shown in Fig. 2, we found that the hardness of the alloy increased sharply when the temperature reached 200 °C, indicating that the solute atoms in the matrix precipitated rapidly. Therefore, a temperature of 200 °C was considered the initial temperature of quenching sensitivity. As the temperature was increased to 310 °C, numerous extremely fine precipitates were observed (Fig. 6), and the hardness reached its peak value (Fig. 2). Afterward, the hardness started to decrease rapidly. In addition, when the temperature was increased to 400 °C, the electrical conductivity of the alloy declined rapidly from its peak value, and the solute atoms in the alloy quickly dissolved back to the matrix.

During the heat treatment process, quenching is necessary to achieve a supersaturated solid solution at room temperature. However, when the solid solution treated specimen is exposed to higher temperatures, the supersaturated solid solution will decompose and precipitate. Thus, the driving force of precipitation is mainly controlled by the degree of supersaturation and the diffusion rate of the solute atoms. At low temperatures, the degree of supersaturation will be very large but the diffusion rate of solute atoms will be low. However, the situation reverses at high temperatures. When the specimens are treated to suitable temperature ranges and maintained for a sufficiently long time, the degree of supersaturation and the diffusion rate of the solute atoms will both be relatively large, facilitating the decomposition of the supersaturated solid and precipitation of the second phase. In this situation, the driving force of precipitation would be reduced during the subsequent aging process, which will also reduce the number of precipitations. As a result, a critical temperature should be observed, beyond which the decomposition of solute atoms will accelerate, resulting in the precipitation of strengthening phase. Below the critical temperature, the precipitation of solute atoms will be inhibited, and the amount of precipitation will be constant even if the alloy is held at this temperature for a long time. The variations in hardness can be regarded as an indication of changes in precipitation behavior. Based on the above analysis, the starting point for the rapid decrease in hardness was considered as the critical temperature (200 °C) and could be treated as the lower limit of the quenching sensitivity temperature range.

With an increase in temperature, the degree of supersaturation was very small but the diffusion rate of the solute atoms was extremely high, which led to the dissolution of solute atoms into the matrix. The precipitation of the second phase was inhibited and the driving force for subsequent precipitation during aging did not decrease, even when the specimen was held at this temperature for a long time. Thus, it was reasonable to conclude that there should be another critical temperature, beyond which the redissolution of the solute atoms would occupy the dominant position, while below which the precipitation of solute atoms played a predominant role. The variations in electrical conductivity were treated as a sign of changes in solute atom behaviors. When the redissolution of solute atoms was apparent, electrical conductivity would decrease accordingly. As a result, the starting point for the rapid decrease in electrical conductivity was considered to be the critical temperature (400 °C) for the upper limit of the quenching sensitivity temperature range. Based on analysis of the hardness and electrical conductivity curves, it was concluded that the quenching sensitivity temperature range of the investigated alloy was 200−400 °C.

4.3 Obtaining quenching sensitivity temperature range by interrupt quenching method

Step 1: Preparing the reference group. The specimens that were cut from the billet were subjected to solid solution treatment at 470 °C for 60 min, and then quenched instantly in water within 2 s. Afterward, the samples were subjected to artificial aging at 120 °C for 24 h. In this case, the hardness was defined as a reference value, which is denoted as A. The schematic diagram showing how to obtain quenching sensitive temperature region via interrupted quenching method is shown in Fig. 8.

Step 2: Designing the holding temperature region. In general, the maximum holding temperature would not exceed the solution temperature, and the minimum temperature would not be lower than the aging temperature. Typically, 30 °C is set as the interval temperature to ensure accurate results and reduce the workload. The solution temperature of the 7055 aluminum alloy is in the range of 450−475 °C; therefore, the upper limit temperature is usually set to be 445 °C. The aging temperature of the 7055 aluminum alloy varied from 120−160 °C (usually, 120 °C is set as the single aging temperature and 160 °C is set as the double aging temperature). Therefore, the holding temperature was designated as 175−445 °C with an interval of 30 °C, and the holding time generally ranged from 1 to 1800 s (usually set to 1, 5, 10, 15, 30, 40, 60, 120, 180, 300, 600, 900, 1200, 1500, and 1800 s).

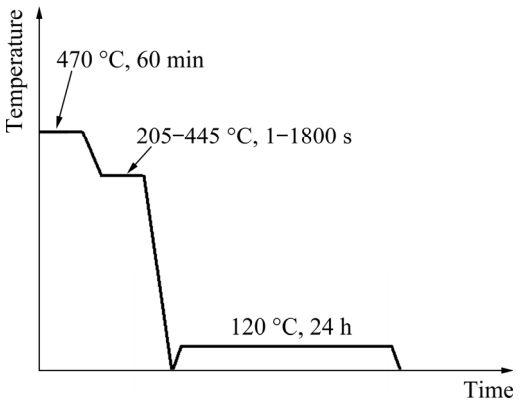

Fig. 8 Schematic diagram showing how to obtain quenching sensitive temperature region via interrupted quenching method

Step 3: Preparing the quenching samples. The samples were prepared according to the holding temperature and time in Step 2. The process of sample preparation was as follows (holding temperature was 445 °C). First, 15 groups of samples were solid solution treated at 470 °C with 1 h in a salt bath furnace. Then, they were transferred quickly (transfer time was less than 2 s) to another salt bath furnace at 445 °C for isothermal treatment. After holding for 1 s, the first group of samples was removed and immediately water quenched (dropped into a room temperature bucket for cooling). After holding for 5 s, the second group was also removed and water quenched. The same procedure was repeated for the next specimen groups according to the process in Step 2 until the last group of samples had a holding time of 1800 s. The samples at the other temperatures were treated according to the same method, and at least 150 samples were used to obtain a sufficient number of results.

Step 4: Artificial aging treatment of the quenched samples. The 150 sample group obtained in Step 3 was treated with artificial aging. All of the samples were placed in a glycerin bath and held at 120 °C for 24 h. After heat-treated preservation, the

samples were water quenched at room temperature, followed by hardness measurements.

Step 5: Drawing of the hardness curves. Drawing the hardness curve was conducted according to the hardness data obtained in Step 4. Using the curve for the sample at 445 °C as an example, the holding time after the solution was obtained was set as the horizontal axis, and the hardness values after aging at 120 °C for 24 h were set as the vertical axis to plot the hardness curve, as shown in Fig. 9(a).

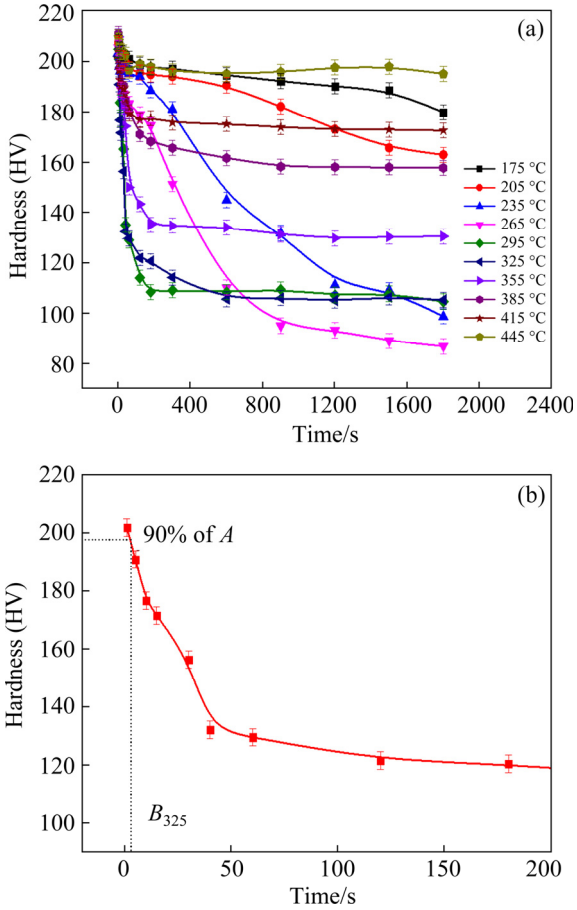

Fig. 9 Hardness value curves with various holding temperatures and holding time after solid solution (a), and hardness value curve at 325°C with different holding time (b) [12]

Step 6: Setting the property degradation coefficient and calculating the corresponding transfer time. Usually, the degrading coefficient is set as the ratio between quenching performance and reference value A. The degradation coefficient can be determined based on actual needs, for example, 90%. After determining the coefficient, the corresponding transfer time was calculated according to each curve, as demonstrated by the hardness curve at 325 °C in Fig. 9(b). When the hardness reached 90% of reference value A, the transfer time was denoted as B_{325}, where the subscript denotes the temperature. The value of B at other temperatures was calculated according to the same methods. Specifically, some values may be infinite, indicating that no matter how long the sample was maintained at that temperature, the final hardness would not drop below 90% of A.

Step 7: Drawing the C Curve for quenching sensitivity and obtaining the high quenching sensitivity region. In the C Curve, as shown in Fig. 10, the holding time was set as the horizontal axis, and the holding temperature was set as the vertical axis. As shown in Fig. 10, when the transfer time was 10 s, the quenching sensitivity temperature range of the alloy was 200−400 °C.

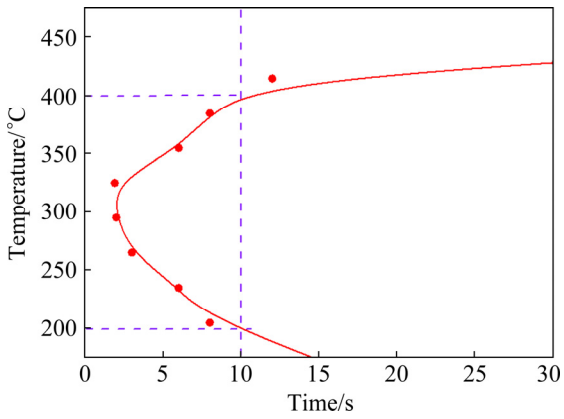

Fig. 10 C Curve for quenching sensitivity

The traditional method requires many steps, numerous test data, the drawing of complex curves, and a huge workload. However, the quenching sensitivity temperature range of the 7XXX aluminum alloy was changed with composition. As a result, this method has limited applications due to its complexity.

By contrast, the method for obtaining the quenching sensitivity temperature range introduced in this work showed both time-saving and resource-saving advantages. The obtained results using the current method were consistent with the results from the traditional interrupted quenching method. This method may also be applicable to other heat-treatable aluminum alloys.

5 Conclusions

(1) The main strengthening phase η' was

formed quickly inside the grains at temperatures between 210 and 310 °C. As the temperature was increased, the η' phase evolved into the η phase, which resulted in the decrease of the strength.

(2) The solute atoms in the homogeneous single-phase supersaturated solid solution could slowly precipitate at 200 °C, and the precipitation rate increased with temperature until 400 °C, at which the electrical conductivity reached its peak value. Above 400 °C, the solute atoms started to redissolve and the electrical conductivity declined.

(3) According to the new ATHT method, the quenching sensitivity temperature range for the current alloy was determined to be 200−400 °C, which was consistent with the results measured by the traditional graded heat preservation method.

Acknowledgments

This work was funded by the National Key Research and Development Plan of China (No. 2020YFA0711104), the Project of State Key Laboratory of High Performance Complex Manufacturing, Central South University, China (No. ZZYJKT2019-04), Scientific Research Initial Funding of Central South University, China (No. 202045001), and the National Natural Science Foundation of China (No. 51901247).

References

[1] LIU Chong-yu, TENG Guang-biao, MA Zong-yi, WEI Li-li, ZHOU Wen-biao, HUANG Hong-feng, QI Hai-quan. Mechanical properties and thermal stability of 7055 Al alloy by minor Sc addition [J]. Rare Metals, 2019, 39: 1−8. https://doi.org/10.1007/s12598-018-1190-z.

[2] LIU Jian, CHENG Yuan-sheng, CHAN S W N, SUNG D. Microstructure and mechanical properties of 7075 aluminum alloy during complex thixoextrusion [J]. Transactions of Nonferrous Metals Society of China, 2020, 30(12): 3173−3182. https://doi.org/10.1016/S1003-6326(20)65452-8.

[3] LI Jia-chen, WU Xiao-dong, LIAO Bin, LIN Xiao-min, CAO Ling-fei. Simulation of low proportion of dynamic recrystallization in 7055 aluminum alloy [J]. Transactions of Nonferrous Metals Society of China, 2021, 31(7): 1902−1915. https://doi.org/10.1016/S1003-6326(21)65625-X.

[4] IEWKITTHAYAKORN I, JANUDOM S, MAHATHANINWONG N, KARRILA S, WANNASIN J. Anodizing parameters for superheated slurry cast 7075 aluminum alloys [J]. Transactions of Nonferrous Metals Society of China, 2019, 29(6): 1200−1210. https://doi.org/10.1016/S1003-6326(19)65027-2.

[5] WANG Qing, ZHAN Li-hua, XU Yong-qian, LIU Chun-hui, ZHAO Xing, XU Ling-zhi, YANG You-liang, CAI Yi-xian. Creep aging behavior of retrogression and re-aged 7150 aluminum alloy [J]. Transactions of Nonferrous Metals Society of China, 2020, 30(10): 2599−2612. https://doi.org/10.1016/S1003-6326(20)65405-X.

[6] SHENG Xiao-fei, LEI Qian, XIAO Zhu, WANG Ming-pu. Hot deformation behavior of a spray-deposited Al−8.31Zn−2.07Mg−2.46Cu−0.12Zr alloy [J]. Metals, 2017, 7(8): 299. https://doi.org/10.3390/met7080299.

[7] LI Yao, XU Guo-fu, PENG Xiao-yan, LIU Shi-Chao, DOU Yu-hai, LIANG Xiao-peng. High temperature mechanical properties and microstructure of die forged Al−5.87Zn−2.07Mg−2.42Cu alloy [J]. Transactions of Nonferrous Metals Society of China, 2020, 30(7): 1771−1779. https://doi.org/10.1016/S1003-6326(20)65337-7.

[8] REYNA-MONTOYA J S, GARCÍA-RENTERÍA M A, CRUZ-HERNÁNDEZ V L, CURIEL-LÓPEZ F F, DZIB-PÉREZ L R, FALCÓN-FRANCO L A. Effect of electro-magnetic interaction on microstructure and corrosion resistance of 7075 aluminium alloy during modified indirect electric arc welding process [J]. Transactions of Nonferrous Metals Society of China, 2019, 29(3): 473−484. https://doi.org/10.1016/S1003-6326(19)64956-3.

[9] LIU L L, PAN Q L, WANG X D, XIONG S W. The effects of aging treatments on mechanical property and corrosion behavior of spray formed 7055 aluminium alloy [J]. Journal of Alloys and Compounds, 2018, 735: 261−276. https://doi.org/10.1016/j.jallcom.2017.11.070.

[10] LIN Hua-qiang, WU Yu-long, LIU Sheng-dan. Impact of initial temper of base metal on microstructure and mechanical properties of friction stir welded AA 7055 alloy [J]. Materials Characterization, 2018, 146: 159−168. https://doi.org/10.1016/j.matchar.2018.09.043.

[11] LIN Hua-qiang, WU Yu-long, LIU Sheng-dan, ZHOU Xiao-rong. Effect of cooling conditions on microstructure and mechanical properties of friction stir welded 7055 aluminium alloy joints [J]. Materials Characterization, 2018, 141: 74−85. https://doi.org/10.1016/j.matchar.2018.04.029.

[12] SHENG Xiao-fei, LEI Qian, XIAO Zhu, WANG Ming-pu. Precipitation behavior and quenching sensitivity of a spray deposited Al−Zn−Mg−Cu−Zr alloy [J]. Materials (Basel), 2017, 10(9): 1100. https://doi.org/10.3390/ma10091100.

[13] PENG Ying-hao, LIU Chong-yu, WEI Li-li, JIANG Hong-jie, GE Zhen-jiang. Quench sensitivity and microstructures of high-Zn-content Al−Zn−Mg−Cu alloys with different Cu contents and Sc addition [J]. Transactions of Nonferrous Metals Society of China, 2021, 31(1): 24−35. https://doi.org/10.1016/S1003-6326(20)65476-0.

[14] GARRIC V, COLAS K, DONNADIEU P, RENOU G, URVOY S, KAPUSTA B. Correlation between quenching rate, mechanical properties and microstructure in thick sections of Al Mg Si(Cu) alloys [J]. Materials Science and Engineering A, 2019, 753: 253−261. https://doi.org/10.1016/j.msea.2019.03.045.

[15] POGATSCHER S, ANTREKOWITSCH H, LEITNER H, PÖSCHMANNC D, ZHANG Z L, UGGOWITZER P J. Influence of interrupted quenching on artificial aging of Al−Mg−Si alloys [J]. Acta Materialia, 2012, 60(11): 4496−4505. https://doi.org/10.1016/j.actamat.2012.04.026.

[16] TZENG Y C, WU C T, LEE S L. The effect of trace Sc on the quench sensitivity of AL−7Si− 0.6Mg alloys [J].

Materials Letters, 2015, 161: 340−342. https://doi.org/10.1016/j.matlet.2015.08.108.

[17] LU Ding-ding, NING Hong, DU Yue, LI Jin-feng, LIU Dan-yang, GUO You-jie, CHEN Yong-lai, ZHANG Xu-hu, YOU Wen, ZHANG Kai, ZHANG Rui-feng. Detailed investigation of quench sensitivity of 2050 Al−Cu−Li alloy by interrupted quenching method and novel end quenching method [J]. Journal of Alloys and Compounds, 2021, 888: 161450. https://doi.org/10.1016/j.jallcom.2021.161450.

[18] ZHANG Yu-xun, YI You-ping, HUANG Shi-quan, DONG Fei, WANG Hui-min. Investigation of the quenching sensitivity of forged 2A14 aluminum alloy by time−temperature−tensile properties diagrams [J]. Journal of Alloys and Compounds, 2017, 728: 1239−1247. https://doi.org/10. 1016/j.jallcom.2017.09.041.

[19] LIU Dan-yang, MA Yun-long, LI Jin-feng, LIU Chen, DU Yue, CHEN Yong-lai, ZHANG Xu-hu, YOU Wen, ZHANG Rui-feng. Quench sensitivity and microstructure evolution of the 2060 Al−Cu−Li alloy with a low Mg content [J]. Materials Characterization, 2021, 177: 111156. https://doi.org/10.1016/j.matchar.2021.111156.

[20] LI Shen-lan, HUANG Zhi-qi, CHEN Wei-peng, LIU Zhi-ming, QI Wen-jun. Quench sensitivity of 6351 aluminum alloy [J]. Transactions of Nonferrous Metals Society of China, 2013, 23(1): 46−52. https://doi.org/10.1016/S1003-6326(13)62427-9.

[21] LIU Shu-hui, WANG Xiang-dong, PAN Qing-lin, LI Meng-jia, YE Ji, LI Kuo, PENG Zhuo-wei, SUN Yu-qiao. Investigation of microstructure evolution and quench sensitivity of Al−Mg−Si−Mn−Cr alloy during isothermal treatment [J]. Journal of Alloys and Compounds, 2020, 826: 154144. https://doi.org/10.1016/j.jallcom.2020.154144.

[22] CHINH N Q, LENDVAI J, PING D H, HONO K. The effect of Cu on mechanical and precipitation properties of Al−Zn−Mg alloys [J]. Journal of Alloys and Compounds, 2004, 378(1/2): 52−60. https://doi.org/10.1016/j.jallcom.2003.11.175.

[23] SHA G, CEREZO A. Early-stage precipitation in Al−Zn−Mg−Cu alloy (7050) [J]. Acta Materialia, 2004, 52(15): 4503−4516. https://doi.org/10.1016/j.actamat.2004.06.025.

[24] SHEN Lei-nuo, LI Zhou, DONG Qi-yi, XIAO Zhu, LI Si, LEI Qian. Microstructure evolution and quench sensitivity of Cu−10Ni−3Al−0.8Si alloy during isothermal treatment [J]. Journal of Materials Research, 2015, 30(5): 736−744. https://doi.org/10.1557/jmr.2015.12.

[25] LI Cheng-bo, HAN Su-qi, LIU Sheng-dan, DENG Yun-lai, ZHANG Xin-ming. Grain structure effect on quench sensitivity of Al−Zn−Mg−Cu−Cr alloy [J]. Transactions of Nonferrous Metals Society of China, 2016, 26(9): 2276−2282. https://doi.org/10.1016/S1003-6326(16)64319-4.

[26] YE Ji, PAN Qing-lin, LI Hang, HUANG Zhi-qi , LIU Ya-ru, WANG Xiang-dong, LI Meng-jia. Quench sensitivity of a 7A46 aluminum alloy [J]. JOM, 2019, 71(6): 2054−2062. https://doi.org/10.1007/s11837-019-03421-y.

[27] PAN T A, TZENG Y C, BOR H Y, LIU K H, LEE S L. Effects of the coherency of Al3Zr on the microstructures and quench sensitivity of Al−Zn−Mg−Cu alloys [J]. Materials Today Communications, 2021, 28: 102611. https://doi.org/10.1016/j.mtcomm.2021.102611.

快速获得 7055 铝合金淬火敏感温度区间的新方法及机理

盛晓菲[1,2]，贺存孝[3,4]，程亚娟[5]，饶晓晓[2]，何国爱[3,4]

1. 中南大学 材料科学与工程学院，长沙 410083；
2. 湖北汽车工业学院 材料科学与工程学院，十堰 442002；
3. 中南大学 轻合金研究所，长沙 410083；
4. 中南大学 高性能复杂制造国家重点实验室，长沙 410083；
5. 广州大学 物理与材料科学学院，广州 510006

摘 要：采用一种省时、节约资源的变温热处理(ATHT)新方法，基于硬度与电导率，获得喷射沉积 7055 铝合金的淬火敏感温度区间。此外，通过透射电子显微镜(TEM)表征 ATHT 期间的显微组织演变。 研究表明，7055 合金的 ATHT 是一个溶质原子随着温度的升高而析出和再溶解的过程。当温度达到 200 ℃时，合金的硬度急剧增加，电导率适当增加。随着温度升高到 400 ℃以上，电导率从峰值迅速下降，表明溶质原子回溶加速，同时，在基体内 η'强化相逐渐转变成 η 平衡相。通过对硬度曲线和电导率曲线的分析，得出当前合金淬火敏感性温度范围为 200~400 ℃，这与传统分级保温法测得的结果一致。

关键词：铝合金；变温热处理；淬火敏感温度区间；显微组织演变

(Edited by Bing YANG)